


# Synergistic interactions between the charge-transport and mechanical properties of the ionic-liquid-based solid polymer electrolytes for solid-state lithium batteries

Ashutosh Agrawal<sup>1,2</sup> | Saeed Yari<sup>1,2</sup> | Hamid Hamed<sup>1,2</sup> | Tom Gouveia<sup>3</sup> | Rongying Lin<sup>3</sup> | Mohammadhosein Safari<sup>1,2,4</sup> 

<sup>1</sup>Institute for Materials Research (IMO-imomec), UHasselt, Hasselt, Belgium

<sup>2</sup>Energyville, Genk, Belgium

<sup>3</sup>Solvionic, Toulouse, France

<sup>4</sup>IMEC Division IMOMECE, Diepenbeek, Belgium

## Correspondence

Mohammadhosein Safari, Institute for Materials Research (IMO-imomec), UHasselt, Martelarenlaan 42, B-3500 Hasselt, Belgium.  
Email: [momo.safari@uhasselt.be](mailto:momo.safari@uhasselt.be)

## Funding information

H2020 LEIT Advanced Materials, Grant/Award Number: 875557

## Abstract

The performance sensitivity of the solid-state lithium cells to the synergistic interactions of the charge-transport and mechanical properties of the electrolyte is well acknowledged in the literature, but the quantitative insights therein are very limited. Here, the charge-transport and mechanical properties of a polymerized ionic-liquid-based solid electrolyte are reported. The transference number and diffusion coefficient of lithium in the concentrated solid electrolyte are measured as a function of concentration and stack pressure. The elastoplastic behavior of the electrolyte is quantified under compression, within a home-made setup, to substantiate the impact of stack pressure on the stability of the Li/electrolyte interface in the symmetric lithium cells. The results spotlight the interaction between the concentration and thickness of the solid electrolyte and the stack pressure in determining the polarization and stability of the solid-state lithium batteries during extended cycling.

## KEYWORDS

battery, diffusion, pressure, solid state, transference

## 1 | INTRODUCTION

All-solid-state batteries are hailed as the holy grail of battery technology due to their inherent safety and wide operating range.<sup>1-3</sup> The nonuniform plating of lithium resulting in dendrite growth and the high interfacial resistance and instability of the Li/electrolyte interface, however, remain to be solved.<sup>4,5</sup> The mossy/dendritic morphology of the lithium/electrolyte interface causes the structural collapse of the cell, and the imperfect interfacial contact leads to high polarization and early

failure of the cell.<sup>4,6,7</sup> A variety of strategies have been proposed to achieve a stable and low impedance interface including interface engineering,<sup>8,9</sup> electrolyte optimization,<sup>10,11</sup> polymer engineering,<sup>12-14</sup> integrated composite electrodes,<sup>15,16</sup> thermally driven Li dendrite suppression,<sup>17,18</sup> and applying stack pressure,<sup>19,20</sup> among others. Major breakthroughs are unlikely until the intricate interactions between the mechanical and charge-transport properties of the solid electrolyte and the lithium/electrolyte interface are understood and holistic steps are taken.

This is an open access article under the terms of the Creative Commons Attribution License, which permits use, distribution and reproduction in any medium, provided the original work is properly cited.

© 2023 The Authors. *Carbon Energy* published by Wenzhou University and John Wiley & Sons Australia, Ltd.

The recent computational literature suggests that the spatially and temporally nonuniform lithium plating and stripping at the electrolyte interface are significantly influenced by the synergistic interactions between the charge transport in the electrolyte and the interfacial charge-transfer kinetics.<sup>21–29</sup> Particularly, the macroscopic physics-based models have provided invaluable insights into the possible constructive role of stack pressure in stabilizing the Li/electrolyte interface. The impact of pressure on the charge-transfer kinetics has been captured by the modified Butler–Volmer kinetic equations.<sup>25–28</sup> The multiscale simulation of the contact mechanics for the lithium/electrolyte interface has provided deep insights into the significance of surface roughness, elastoplasticity, and creep in preserving a low-impedance interface and the benefits of stack compression.<sup>28</sup> The charge-transport properties of the solid electrolyte have been incorporated into the modified-ohms law for the ionic current in the bulk of the electrolyte parametrized with the lithium transference number, ionic conductivity, and diffusion coefficient.<sup>30–33</sup> Stress-driven ionic current in the bulk of single-ion conductor electrolytes has been shown effective in mitigating the irregular deposition of lithium.<sup>27</sup>

The current experimental literature is rich in reports about the impact of stack pressure, temperature, and current density on the performance of Li solid-state cells.<sup>19,34–37</sup> There is, however, very limited literature on the quantitative analysis and measurement of the mechanical and transport properties of the solid electrolytes and their synergistic effects on the stability of the Li/electrolyte interface.

In this work, we measure the stress/strain behavior and a complete set of charge-transport parameters for a solid-polymer electrolyte (SPE), that is, [(LiTFSI in EMI TFSI): PolyDDA TFSI], as a function of compressive pressure, lithium concentration, and electrolyte thickness. These parameters are then used for quantitative analysis of the polarization and stability of the Li/electrolyte interface in Li|SPE|Li cells during storage and continuous cycling.

## 2 | EXPERIMENTAL SECTION

### 2.1 | Materials

The SPEs with Li - bis(trifluoromethanesulfonyl)imide (Li TFSI) salt concentrations  $x$  of = 0.8, 1, and 1.2 M were prepared with a composition of [( $x$ M LiTFSI in EMI TFSI): PolyDDA TFSI] [60:40 wt%] by Solvionic. To do so, first the polymer electrolyte solutions were prepared

by dissolving Li TFSI, EMI TFSI, and polydiallyldimethylammonium (polyDDA) TFSI in acetonitrile. The free-standing SPE sheets (Figure S10a) of various thicknesses were produced by casting the as-prepared polymer electrolyte solutions using blade coating (doctor blade) in ambient conditions. Evaporation of the solvent was done by leaving the film in ambient conditions for 30 min. Afterward, the membrane was dried under vacuum at 80°C. All the electrolyte components were weighed in their dry state, under less than 10 ppm of water and 1 ppm of oxygen conditions. The lithium electrodes used in the preparation of the cells were punched from the Li foils with a thickness of 200  $\mu\text{m}$ .

### 2.2 | Characterizations

An electrochemical pressure-cell setup with force and displacement sensors was designed and manufactured in-house to measure the stress–strain behavior of the solid electrolyte samples and to cycle the Li|SPE|Li cells under controlled pressure (Figure S10b). The setup features an air-tight split coin cell with one moving part attached to the current collector, which can be pressurized. HBK's force transducer (resolution of 0.1 kPa and accuracy of 20 kPa) and Keyence's cylinder contact type high-precision displacement sensor (resolution of 0.1  $\mu\text{m}$  and accuracy of 1  $\mu\text{m}$ ) head were used to monitor the pressure and strain, respectively. The cells were assembled inside an argon-filled glovebox (Mbraun, O<sub>2</sub>, and H<sub>2</sub>O below 1 ppm). All the measurements were carried out at 25°C and the force and displacement sensors were calibrated before the tests.

#### 2.2.1 | Electrochemical

Li|SPE|Li cells assembled with SPEs of different thicknesses (100 and 300  $\mu\text{m}$ ) and salt concentrations (0.8 and 1.2 M) were cycled galvanostatically at different current densities (0.05 and 0.1 mA/cm<sup>2</sup>) and stack pressures (1, 2.5, and 5 MPa). The electrochemical cycles conducted with Bio-Logic (VMP3) consisted of 1 h plating and stripping intervals continuously repeated until short-circuit or spike in the voltage. The electrochemical impedance spectra of the symmetric cells were recorded over the frequency range of 1 MHz–100 mHz with an excitation amplitude of 10 mV. The charge-transport properties including the lithium diffusion coefficient and transference number and the ionic conductivity of the solid electrolyte samples were measured following the orthogonal experiments of Newman. The transference number was also measured using the more conventional

method of Bruce–Vincent for comparison. The details of the two methods can be found in the Supporting Information.

### 2.2.2 | Mechanical

The pressure-cell setup was used to obtain the compressive stress–strain curves for the SPE samples with different thicknesses and concentrations. Compression tests were performed with SPEs with diameter of 6 mm and thicknesses of 50, 100, 300, 400, and 500  $\mu\text{m}$ . The SPEs of 400 and 500  $\mu\text{m}$  were prepared by stacking the 100 and 300  $\mu\text{m}$ -thick samples. All samples were compressed to 50% of the thickness (i.e., 0.5 strain) a few micrometers at a time to keep the average strain rates around 10–2  $\text{s}^{-1}$ . As such, the SPEs with thickness of 50, 100, and 300  $\mu\text{m}$  were compressed with a rate of 0.5, 1, and 3  $\mu\text{m/s}$ , respectively.

## 3 | RESULTS

The stability and contact for the SPE/Li interface were followed for 200 h in the absence of any electrochemical load by recording the electrochemical impedance spectroscopy (EIS) spectra of Li|SPE|Li cells every 2 h at 25°C (Figure S1). The charge-transfer resistance ( $R$ ) at the Li/electrolyte interface evolves with a peculiar dynamic during the ~250 h of the storage period after the cell assembly (Figure 1A,B). A few important observations are noteworthy. First, the variation in  $R$  is nonmonotonic and the resistance value reaches a maximum and stabilizes to a minimum only toward the end of the rest period (>150 h). Second, the stack pressure demonstrates a constructive impact on the shortening of the stabilization time and decreasing the  $R$ . The stable resistance values are on average higher at 1.2 M relative to the 0.8 M salt concentration. The resistance values decline with

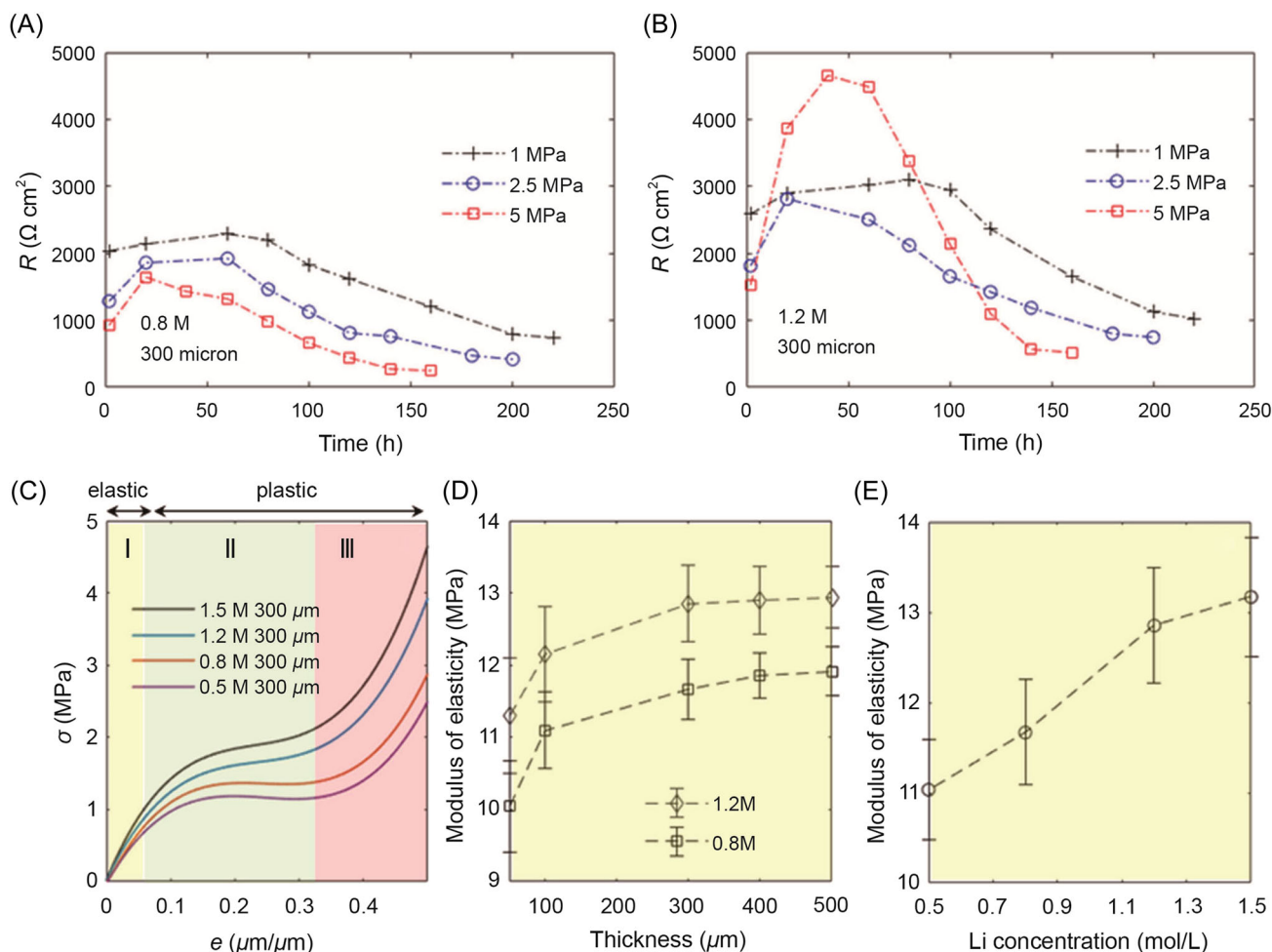


**FIGURE 1** Evolution of the charge-transfer resistance for the Li|SPE|Li cells during the ~250 h of the storage period after cell assembly and before the start of cycling was measured by recording the EIS spectra every 2 h at 25°C (Figure S1) at different pressures and for concentrations of (A) 0.8 M and (B) 1.2 M and (C) compressive stress–strain curves for the SPE samples with different concentrations and thicknesses to approximate the effective modulus of elasticity as a function of (D) thickness at two concentrations; (E) concentration at SPE thickness of 300  $\mu\text{m}$ .

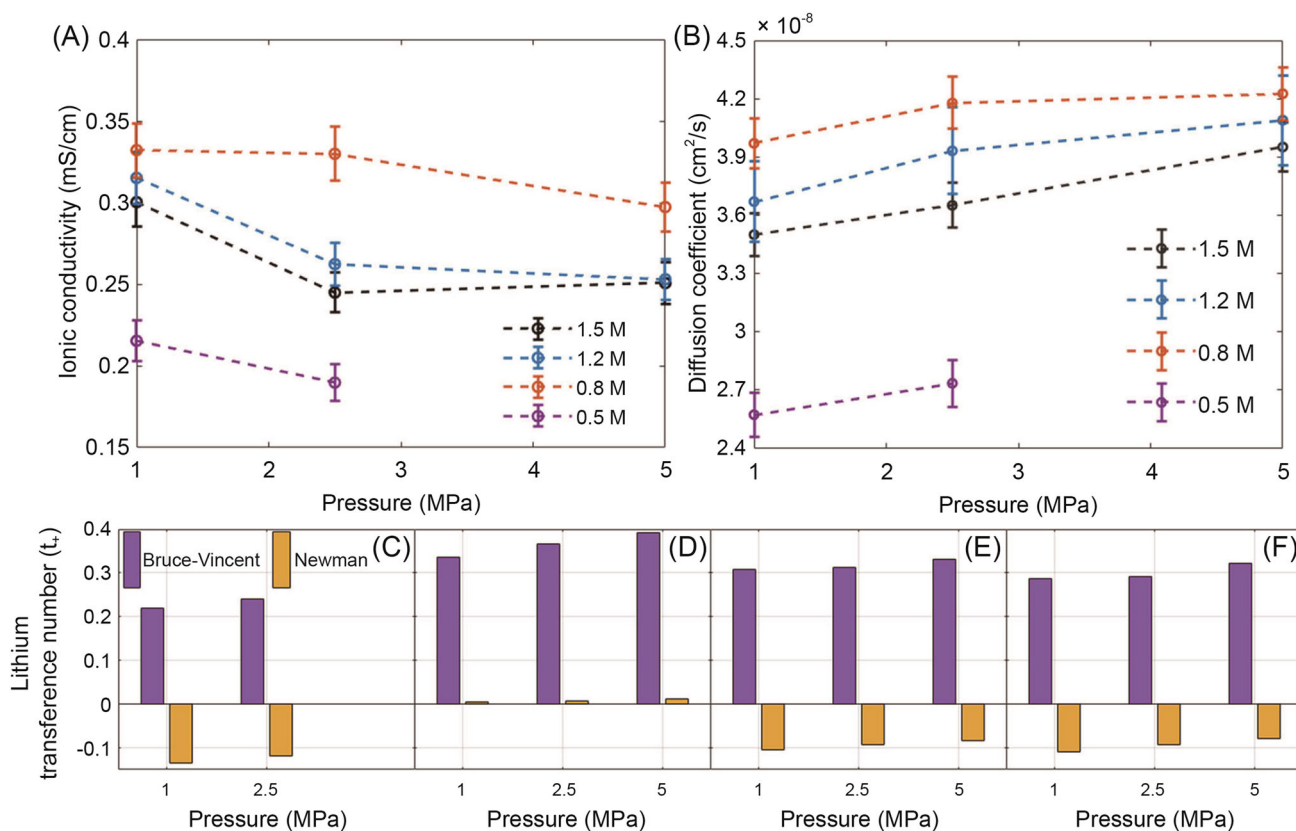


**FIGURE 2** (A) Ionic conductivity, (B) diffusion coefficient, and (C–F) lithium transference number for the SPE samples with 300  $\mu\text{m}$  thickness as a function of electrolyte concentration and pressure. The transference values from the Bruce–Vincent method are superimposed for comparison. It is noteworthy that for the sample with 0.5 M Li concentration, the SPE breaks under 5 MPa and as such the data are only presented up to 2.5 MPa at this concentration.

approximate rates of 17% and 12.5%  $\text{MPa}^{-1}$  at 0.8 and 1.2 M salt concentrations, respectively. The stabilization time is decreased by 27%, regardless of the salt concentration, when the stack pressure is increased from 1 to 5 MPa. Similar trends are observed at 0.5 and 1.5 M concentrations (Figure S2). The observed impedance trends suggest that there are two main competing mechanisms going on in parallel. The first is the passivation of the lithium as a result of the side reactions between the electrolyte and lithium metal, and the second is the continuous interfacial wetting between the electrode and the electrolyte. Initial hours are dominated by the side reactions, which cause an increase in the impedance, whereas interfacial bonding/wetting starts dominating at later stages, decreasing the overall impedance (Figure S1). The latter is governed by the mechanical properties of the bulk and interface.

During cycling, the SPE undergoes cyclic compressive stress that steadily increases as unwanted reactions on the electrodes create irreversible volume changes.<sup>20</sup> Therefore, it is of vital importance to study the stress–strain behavior of the SPEs under compression.

The engineering stress–strain plots for the SPEs with four different concentrations of 0.5, 0.8, 1.2, and 1.5 M were obtained under compression (Figure 1C). The elastic (zone I) and plastic (zone II and III) ranges are distinguished by the yield starting at  $\sim 1$ –1.5 MPa above which the strain continues to increase at a constant stress. This range of yield stress is quite low compared with that in the reports for lithium, that is., 15–105 MPa,<sup>28,38</sup> and highlights the potential benefit of the solid electrolyte's creep in promoting a conformal contact between the lithium and electrolyte at lower stack pressures. At strains above 30%, the strain hardening is observed (zone III) that might possibly originate from the reorientation of the polymer chains<sup>39</sup> or/and the barrelling effect induced by the frictional forces.<sup>39,40</sup> The modulus of elasticity ( $E$ ) for the solid electrolyte samples shows a nonnegligible sensitivity to the thickness (Figure 1D) and salt concentration (Figure 1E). For instance, the electrolytes with a 1.2 M concentration, on average, have a  $\sim 10\%$  higher modulus compared with the samples with a concentration of 0.8 M. The value of  $E$  increases with an average rate of 3%

and  $4\% \mu\text{m}^{-1}$  at salt concentrations of 1.2 and 0.8 M, respectively, when the thickness of the electrolyte is increased from 50 to 500  $\mu\text{m}$ . At lower thicknesses, the mechanical properties might deteriorate due to edge effects and low surface-to-volume ratio. The SPE's modulus of elasticity increases with an average rate of  $20\% \text{M}^{-1}$  when the lithium concentration increases in the range of 0.5 to 1.5 M (Figure 1E).

The charge-transport properties of the solid electrolytes were measured at different pressures and electrolyte concentrations (Figure 2). In the solid electrolyte literature, it is the ionic conductivity that is mostly reported and the measurement of a complete set of charge-transport properties including the diffusion coefficient and transference number is exceptional. The quantitative information about the latter two properties is crucial, however, to understand and optimize the performance of the solid-state batteries made with a nonsingle ionic conductor as the electrolyte. Li transference number ( $t_+$ ) is defined as the fraction of the ionic current carried by the lithium ions in the electrolyte in the absence of concentration gradients.<sup>30</sup> Any deviation from  $t_+ = 1$  signifies the contribution of diffusion phenomena in the transport of lithium between the two electrodes with the consequence of a concentration gradient build-up in the electrolyte. To date,  $t_+$  has been measured for the solid electrolytes mainly by the method of Bruce–Vincent.<sup>41</sup> This method, however, is limited to the ideal and dilute electrolytes.<sup>31–33</sup> Newman and co-workers developed in 1995 a set of coupled orthogonal experiments to measure the transport properties of the concentrated electrolytes and showcased it for an SPE. This method, however, is rarely used in the solid electrolyte literature.<sup>32,33</sup>

In the more concentrated electrolytes (e.g., at 1.2 M), the average ionic conductivity (0.28 mS/cm) is  $\sim 12\%$  lower relative to that of the electrolyte with 0.8 M concentration (0.32 mS/cm) (Figure 2A). The increased pressure, from 1 to 5 MPa, reveals a negative impact on the ionic conductivity with a decline rate of 2.5% and 5%  $\text{MPa}^{-1}$  at 0.8 and 1.2 M concentrations, respectively. Further increase of stack pressure beyond 5 MPa and up to 7.5 MPa slightly increases the ionic conductivity for the SPEs with concentrations higher than 0.5 M (Figure S3). The SPE with 0.5 M concentration exhibits the lowest ionic conductivity (0.2 mS/cm) in the concentration and pressure ranges investigated in this study (Figure 2A). Similar to other concentrations, the pressure increase has a negative effect on the ionic conductivity at 0.5 M. The variation of ionic conductivity with salt concentration exhibits various trends depending on the stack pressure (Figure S4). Particularly, unlike the conventional liquid electrolytes in

lithium-ion batteries, the usual conductivity peak found at 1 M is absent at higher stack pressures, which highlights the necessity of a comprehensive sensitivity analysis including the pressure and concentration in the formulation of the SPEs. The highest lithium diffusion coefficient, similar to the ionic conductivity, is observed for the SPE with 0.8 M concentration and the lowest diffusion coefficient belongs to the SPE with 0.5 M concentration ( $2.5 \times 10^{-8} \text{cm}^2/\text{s}$ ). The diffusion coefficient is on average 5% and 10% higher at 0.8 M ( $4.1 \times 10^{-8} \text{cm}^2/\text{s}$ ) compared with the 1.2 M ( $3.9 \times 10^{-8} \text{cm}^2/\text{s}$ ) and 1.5 M ( $3.7 \times 10^{-8} \text{cm}^2/\text{s}$ ), respectively (Figure 2B). The higher pressure, however, unlike the ionic conductivity, slightly enhances the diffusion with the constructive impacts of 1.5%  $\text{MPa}^{-1}$  at 0.8 M and 2.8%  $\text{MPa}^{-1}$  at higher concentrations.

As expected, we observe a significant difference between the values of  $t_+$  measured from the Newman and Bruce–Vincent methods (Figure 2C–F). The latter method determines one order of magnitude higher transference values (0.34) for the lithium ion compared with the Newman method ( $-0.04$ ), which spotlights the very concentrated and nonideal behavior of our solid electrolytes in the concentration range of 0.5–1.5 M. Regardless of the method, higher  $t_+$  is obtained at higher pressures. For instance, for the Newman method,  $t_+$  shows a sensitivity of  $\sim 16\%$  and 5%  $\text{MPa}^{-1}$  at 0.8 and 1.2 M salt concentrations, respectively. The transference number is decreased at higher salt concentrations (1.2 vs. 0.8 M) up to 27- and 1.3-fold according to the Newman and Bruce–Vincent methods, respectively. A similar concentration dependence trend to those of conductivity and diffusion is observed for the lithium transference number where the smallest  $t_+$  is seen at a concentration of 0.5 M.

The voltage–time profiles of the symmetric Li cells during constant-current cycling at 0.05 (Figure 3A) and 0.1  $\text{mA}/\text{cm}^2$  (Figure 3B) were recorded with (dis)charge periods of 1 h until cell failure, that is, reaching the safety cut-off voltage ( $\pm 5 \text{V}$ ) or short-circuit (Figure S5). The increase of polarization and time-to-failure (TTF) of the cells display a clear correlation with the pressure (Figure 3). The TTF is postponed by  $\sim 40\% \text{MPa}^{-1}$  when the pressure is increased from 1 to 5 MPa under both low and high current cycling. The resistance build-up is up to three times faster at higher currents regardless of the pressure. Cycling at a higher pressure demonstrates a clear advantage for the diminution of the resistance rise in the cells. An effective rate of resistance (ROR) build-up can be approximated based on the cell voltage and accumulative charge throughput during the cycling (Figure S6). At a lower current, the average ROR decreases from 8.9 to 1  $\Omega \text{h}^{-1}$  by increasing the pressure from 1 to 5 MPa (Figure 3A). A similar trend holds true at

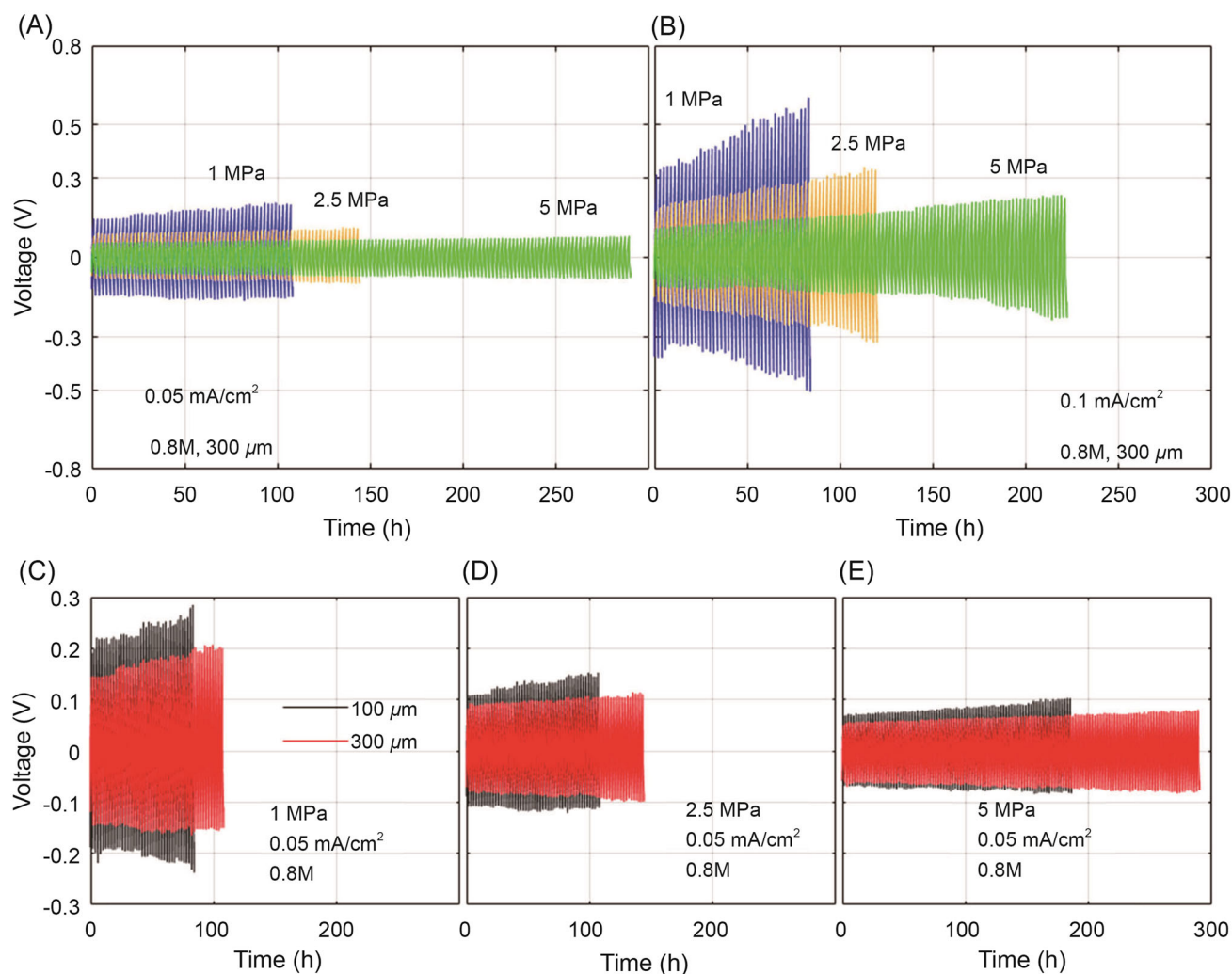


**FIGURE 3** Impact of pressure on the voltage profiles for Li/SPE/Li symmetric coin cells cycled at room temperature with an SPE thickness of 300  $\mu\text{m}$  and concentration of 0.8 M at the current density of (A) 0.05  $\text{mA}/\text{cm}^2$ , (B) 0.1  $\text{mA}/\text{cm}^2$ . The voltage profiles were compared between the cells with SPE thickness of 100  $\mu\text{m}$  (black) and 300  $\mu\text{m}$  (red) cycled with 0.05  $\text{mA}/\text{cm}^2$  at different pressures of (C) 1 MPa, (D) 2.5 MPa, and (E) 5 MPa.

higher currents with a reduction of ROR from 30.6 to 6.9  $\Omega\text{h}^{-1}$  (Figure 3B). These results suggest that the pressure can suppress the rise in the internal resistance of the cell by a factor of  $\sim 20\% \text{ MPa}^{-1}$ . The cells with the 1.2 M electrolyte (Figure S7) share the same general trends as the ones at 0.8 M with respect to the polarization and its sensitivity to the pressure. The electrolyte thickness has a noteworthy impact on the failure time of the cells (Figure 3C,D). The TTF for cells with the 300  $\mu\text{m}$  electrolyte is extended by  $\sim 30\%$ , 33%, and 57% at pressures 1, 2.5, and 5 MPa, respectively, in comparison to the cells with a 100  $\mu\text{m}$  electrolyte. This observation is rather intuitive in view of the longer path for the dendrites to short out through a thicker electrolyte. The polarization of the cell is, however, perversely lower for the cell with a thicker electrolyte irrespective of the pressure (Figure 3C,D). This

counterintuitive observation suggests that the polarization in our cells is not dominated by the long-range transport of the charged species through the bulk of the electrolyte and that the interfacial charge-transfer kinetics has a significant role. This is in line with the lower charge-transfer resistance measured via EIS for the thicker solid electrolytes at the start of the cycling (Figure S8).

## 4 | DISCUSSION

In a symmetric binary electrolyte with monovalent cations and anions, the electrochemical potential of the electrolyte ( $\mu_e$ ) and anions ( $\mu_-$ ), the cationic transference number ( $t_+$ ), and ionic current density ( $i$ ) are correlated according to the concentrated solution theory<sup>30</sup>

$$-\nabla\mu_- = -\frac{F}{\kappa}i - t_+\nabla\mu_e, \quad (1)$$

where  $F$  is the Faraday constant and  $\kappa$  is the electrolyte conductivity. The electrochemical potential of the cation and anion might be arbitrarily explained by the three distinct contributions from the chemical potential ( $\mu_i^0$ ), the electrical state of the electrolyte ( $\Phi$ ), and the hydrostatic stress ( $\sigma$ ), according to the following equations:

$$\mu_+ = \mu_+^0 + F\Phi - \lambda^+\sigma, \quad (2)$$

$$\mu_- = \mu_-^0 - F\Phi - \lambda^-\sigma, \quad (3)$$

where  $\lambda^+$  and  $\lambda^-$  stand for the partial molar volumes of the cations and anions, respectively, in the electrolyte with a negative sign convention for the compressive stress.

Equations (1)–(3) can be further combined to obtain a modified Ohms law for the ionic current inside the electrolyte considering the effect of stress and electrolyte concentration ( $c$ )

$$i = -\kappa\nabla\Phi + \kappa\omega\frac{RT}{F}\nabla\ln c + \kappa\frac{(t_+\lambda^+ - t_-\lambda^-)}{F}\nabla\sigma, \quad (4)$$

where  $\omega$  is a parameter depending on the thermodynamics and transport behavior of the electrolyte

$$\omega = t_-\left(1 + \frac{\partial\ln f_-}{\partial\ln c}\right) - t_+\left(1 + \frac{\partial\ln f_+}{\partial\ln c}\right), \quad (5)$$

where  $f_+$  and  $f_-$  stand for the molar ionic activity coefficients of cations and anions, respectively.

The stress-driven current (last term in Equation 4) can promote the uniform deposition of lithium by directing the flow of lithium ions away from the locations under higher compression, that is, the lithium protrusions, toward the pores and valleys.<sup>26,27</sup> This constructive effect, however, depends on the transference number and the partial molar volumes of the lithium ion and the counter ion in the electrolyte. The stress-driven current enhances the uniformity of lithium deposition when  $t_+\lambda^+ - t_-\lambda^- > 0$  and otherwise can even exacerbate the irregular deposition of lithium and dendritic growth. This is a synergistic interaction between the mechanical and transport aspects of the Li/electrolyte interface and it highlights the significance of developing electrolytes with higher lithium transference numbers. This can partly explain the continuous rise of polarization during cycling even under high compression on account of the very low  $t_+$  in the solid electrolytes used in this work. The very

small values of  $t_+$  in our electrolytes reflect the presence of the negatively charged  $[\text{Li}_x(\text{TFSI})_y]^{x-y}$  clusters, which have been extensively reported in previous computational and experimental studies.<sup>42–44</sup> These clusters have a sufficiently long lifetime, which makes them relevant for Li-ion transport via a vehicular transport mechanism.<sup>43</sup>

The efficiency of the compression approach to enhance the stability of the lithium–electrolyte interface depends on the static and dynamic mechanical properties of both lithium and solid electrolytes. The creep of lithium and solid electrolytes can enhance the uniformity of the interface when one or both yield under pressure. Considering the considerably higher yield strength of the Li metal (~15–105 MPa)<sup>38</sup> compared with the yield stress of our samples (<2 MPa), the flow of the solid electrolyte seems to relatively dominate the observed enhancement of contact in our cells (Figure 1). The stress distribution in the electrolyte bulk and at the interface with Li influences not only the dynamics of the creep phenomena but also the ionic current (Equation 4) distribution in the cell. In this regard, not only the intrinsic mechanical properties of the solid electrolyte (e.g., modulus of elasticity) but also the electrolyte thickness will impact the dynamics of current and stress distribution in the cell. This might explain the lower polarization and stability of the thicker electrolytes during cycling (Figure 3C–E). The effect of salt concentration on the charge-transport properties of the liquid electrolytes is well understood<sup>30</sup> from the perspective of the ion–ion interactions in a concentrated solution. The nonnegligible role of stress/strain in the solid electrolytes, however, lends more significance to the role of salt concentration because of its additional impact on the mechanical properties of the solid electrolyte (Figure 1D). In this regard, the lower polarization observed for the cells with the electrolyte formulation of 0.8 M, relative to the more concentrated electrolytes, might be partly credited to the lower effective modulus of elasticity and yield stress of 0.8 M samples facilitating the creep and enhancing the Li/electrolyte contact. The complex charge-transport behavior of the SPE is not only reflected in the nonmonotonic variations of  $\kappa$ ,  $D$ , and  $t_+$  with the concentration in the range of 0.5 to 1.5 M (Figures 2 and S9) but also in the nonuniformity of variation trends among  $\kappa$ ,  $D$ , and  $t_+$  in response to the change of stack pressure. Such complexities might be qualitatively explained by the nonlinear variations of the effective concentration of charge carriers ( $c$ ) and the binary diffusion coefficients ( $\mathcal{D}_j$ ) in the context of a simplified framework such as the (moderate) dilute solution theory for a binary electrolyte and after neglecting the thermodynamic correction factor for the salt diffusion coefficient<sup>30</sup>

$$\kappa = \frac{F^2}{RT}(\mathcal{D}_+ + \mathcal{D}_-)c, \quad (6)$$

$$D = \frac{2\mathcal{D}_+\mathcal{D}_-}{\mathcal{D}_+ + \mathcal{D}_-}, \quad (7)$$

$$t_+ = \frac{\mathcal{D}_+}{\mathcal{D}_+ + \mathcal{D}_-}. \quad (8)$$

One might speculate that the stack pressure has a positive and negative correlation coefficient with  $\mathcal{D}_+$  and  $\mathcal{D}_-$ , respectively, with a higher pressure sensitivity for  $\mathcal{D}_-$ . Such a hypothesis can correctly explain (Equations 6–8) the experimental trends for the variations of  $\kappa$ ,  $D$ , and  $t_+$  with pressure (Figure 2) where the simultaneous rise of the diffusion coefficient and lithium transference number is concurrent with the decline of ionic conductivity at a given concentration. Such an opposite sensitivity of the  $\text{Li}^+$  and its counter ion's mobility to the pressure might be understood in the context of the smaller size of  $\text{Li}^+$  relative to  $\text{TFSI}^-$  and the confinement effects reported for the ionic liquids.<sup>45–49</sup> The confinement effect considers a deviation of the transport properties of an ionic liquid from its bulk values when placed in a submicron or nanoscale confinement as a result of a complex interplay between competing effects involving local concentrations, ionic mobility hindrance, and dynamical molecular cross-interactions. In this regard, the compression of the SPE seems to induce a mobility enhancement and hindrance for the lithium and its counter ion, respectively, which needs further investigation beyond the scope of the current research.

## 5 | CONCLUSIONS

In this work, a solid-polymerized ionic-liquid electrolyte was used as a model experimental system to shed some light on the complex interactions among the charge-transport and mechanical properties of an SPE for application in lithium batteries. The mechanical and transport properties of the electrolyte were showcased to be sensitive to the electrolyte concentration, thicknesses, and stack pressure. The polarization and stability behavior of the symmetric Li cells under compression and over continuous cycling were discussed and quantified in view of the synergistic interactions between the charge-transport and mechanical parameters in the bulk of the electrolyte and the contact elastoplasticity at the Li/electrolyte interface. The significant deviation between the lithium transference values measured via the conventional method of Bruce–Vincent and Newman was highlighted for the concentrated solid

electrolytes and its implications were discussed for the design and optimization of the nonsingle ionic conductors. Our findings highlight the need for a holistic approach in the design of SPEs in which the interactions among the lithium transference number and mechanical properties of the electrolyte are accounted for by proper optimization of the salt concentration, electrolyte thickness, and stack pressure. The results suggest that the SPE at 0.8 M lithium concentration and with a stack pressure of 5 MPa results in the best performance of Li/SPE/Li cells. Further research needs to concentrate on the integration of the solid electrolyte in the Li-insertion porous electrodes to optimize the intimate contact between the active-material particles and SPE in thick porous electrodes.

## ACKNOWLEDGMENTS

This work was supported by funding from the European Union's Horizon 2020 research and innovation program for the Solidify project under grant agreement No. 875557.

## CONFLICT OF INTEREST STATEMENT

The authors declare no conflict of interest.

## ORCID

Mohammadhosein Safari  <http://orcid.org/0000-0003-0633-731X>

## REFERENCES

1. Kalthoff J, Eshetu GG, Bresser D, Passerini S. Safer electrolytes for lithium-ion batteries: state of the art and perspectives. *ChemSusChem*. 2015;8(13):2154–2175.
2. Judez X, Eshetu GG, Li C, Rodriguez-Martinez LM, Zhang H, Armand M. Opportunities for rechargeable solid-state batteries based on Li-intercalation cathodes. *Joule*. 2018;2(11):2208–2224.
3. Lin YY, Yong AXB, Gustafson WJ, et al. Toward design of cation transport in solid-state battery electrolytes: structure-dynamics relationships. *Curr Opin Solid State Mater Sci*. 2020;24(6):100875.
4. Tripathi AM, Su WN, Hwang BJ. In situ analytical techniques for battery interface analysis. *Chem Soc Rev*. 2018;47(3):736–851.
5. Zhao Q, Stalin S, Archer LA. Stabilizing metal battery anodes through the design of solid electrolyte interphases. *Joule*. 2021;5(5):1119–1142.
6. Paul PP, Chen BR, Langevin SA, Dufek EJ, Nelson Weker J, Ko JS. Interfaces in all solid state Li-metal batteries: a review on instabilities, stabilization strategies, and scalability. *Energy Storage Mater*. 2022;45:969–1001.
7. Cao D, Sun X, Li Q, Natan A, Xiang P, Zhu H. Lithium dendrite in all-solid-state batteries: growth mechanisms, suppression strategies, and characterizations. *Matter*. 2020;3(1):57–94.



8. Dai J, Yang C, Wang C, Pastel G, Hu L. Interface engineering for garnet-based solid-state lithium-metal batteries: materials, structures, and characterization. *Adv Mater.* 2018;30(48):1802068.
9. Van den Broek J, Afyon S, Rupp JLM. Interface-engineered all-solid-state Li-ion batteries based on garnet-type fast Li<sup>+</sup> conductors. *Adv Energy Mater.* 2016;6(19):1600736.
10. Wang S, Zhang Y, Zhang X, et al. High-conductivity argyrodite Li<sub>6</sub>PS<sub>5</sub>Cl solid electrolytes prepared via optimized sintering processes for all-solid-state lithium-sulfur batteries. *ACS Appl Mater Interfaces.* 2018;10(49):42279-42285.
11. Li J, Zhu K, Wang J, et al. Optimisation of conductivity of PEO/PVDF-based solid polymer electrolytes in all-solid-state Li-ion batteries. *Mater Technol.* 2022;37(4):240-247.
12. Wang Z, Shen L, Deng S, Cui P, Yao X. 10 μm-thick high-strength solid polymer electrolytes with excellent interface compatibility for flexible all-solid-state lithium-metal batteries. *Adv Mater.* 2021;33(25):2100353.
13. Xu F, Deng S, Guo Q, Zhou D, Yao X. Quasi-ionic liquid enabling single-phase poly (vinylidene fluoride)-based polymer electrolytes for solid-state LiNi<sub>0.6</sub>Co<sub>0.2</sub>Mn<sub>0.2</sub>O<sub>2</sub>|| Li batteries with rigid-flexible coupling interphase. *Small Methods.* 2021;5(7):2100262.
14. Wang Z, Guo Q, Jiang R, et al. Porous poly (vinylidene fluoride) supported three-dimensional poly (ethylene glycol) thin solid polymer electrolyte for flexible high temperature all-solid-state lithium metal batteries. *Chem Eng J.* 2022;435:135106.
15. Kim K, Park J, Jeong G, et al. Rational design of a composite electrode to realize a high-performance all-solid-state battery. *ChemSusChem.* 2019;12(12):2637-2643.
16. Baggetto L, Niessen RAH, Roozeboom F, Notten PHL. High energy density all-solid-state batteries: a challenging concept towards 3D integration. *Adv Funct Mater.* 2008;18(7):1057-1066.
17. Wang Z, Zhang Y, Zhang P, et al. Thermally rearranged covalent organic framework with flame-retardancy as a high safety Li-ion solid electrolyte. *eScience.* 2022;2(3):311-318.
18. Li Z, Xie HX, Zhang XY, Guo X. In situ thermally polymerized solid composite electrolytes with a broad electrochemical window for all-solid-state lithium metal batteries. *J Mater Chem A.* 2020;8(7):3892-3900.
19. Doux JM, Nguyen H, Tan DHS, et al. Stack pressure considerations for room-temperature all-solid-state lithium metal batteries. *Adv Energy Mater.* 2020;10(1):1903253.
20. Koerver R, Zhang W, De Biasi L, et al. Chemo-mechanical expansion of lithium electrode materials – on the route to mechanically optimized all-solid-state batteries. *Energy Environ Sci.* 2018;11(8):2142-2158.
21. Yamakawa S, Ohta S, Kobayashi T. Effect of positive electrode microstructure in all-solid-state lithium-ion battery on high-rate discharge capability. *Solid State Ionics.* 2020;344:115079.
22. Sun Z-T, Bo S-H. Understanding electro-mechanical-thermal coupling in solid-state lithium metal batteries via phase-field modeling. *J Mater Res.* 2022;37(19):3130-3145.
23. Hao F, Mukherjee PP. Mesoscale analysis of the electrolyte-electrode interface in all-solid-state Li-ion batteries. *J Electrochem Soc.* 2018;165(9):A1857-A1864.
24. Nolan AM, Zhu Y, He X, Bai Q, Mo Y. Computation-accelerated design of materials and interfaces for all-solid-state lithium-ion batteries. *Joule.* 2018;2(10):2016-2046.
25. Monroe C, Newman J. The impact of elastic deformation on deposition kinetics at lithium/polymer interfaces. *J Electrochem Soc.* 2005;152(2):A396.
26. Barai P, Higa K, Srinivasan V. Impact of external pressure and electrolyte transport properties on lithium dendrite growth. *J Electrochem Soc.* 2018;165(11):A2654-A2666.
27. Mistry A, Mukherjee PP. Molar volume mismatch: a malefactor for irregular metallic electrodeposition with solid electrolytes. *J Electrochem Soc.* 2020;167(8):082510.
28. Zhang X, Wang QJ, Harrison KL, Roberts SA, Harris SJ. Pressure-driven interface evolution in solid-state lithium metal batteries. *Cell Rep Phys Sci.* 2020;1(2):100012.
29. Bistri D, Afshar A, Di Leo CV. Modeling the chemo-mechanical behavior of all-solid-state batteries: a review. *Meccanica.* 2021;56(6):1523-1554.
30. Newman J. *Electrochemical Systems.* Wiley; 2004.
31. Ma Y, Doyle M, Fuller TF, Doeff MM, De Jonghe LC, Newman J. The measurement of a complete set of transport properties for a concentrated solid polymer electrolyte solution. *J Electrochem Soc.* 1995;142(6):1859-1868.
32. Balsara NP, Newman J. Relationship between steady-state current in symmetric cells and transference number of electrolytes comprising univalent and multivalent ions. *J Electrochem Soc.* 2015;162(14):A2720-A2722.
33. Gao KW, Fang C, Halat DM, Mistry A, Newman J, Balsara NP. The transference number. *Energy Environ Mater.* 2022;5(2):366-369.
34. Boaretto N, Garbayo I, Valiyaveetil-SobhanRaj S, et al. Lithium solid-state batteries: state-of-the-art and challenges for materials, interfaces and processing. *J Power Sources.* 2021;502:229919.
35. Krauskopf T, Richter FH, Zeier WG, Janek J. Physicochemical concepts of the lithium metal anode in solid-state batteries. *Chem Rev.* 2020;120(15):7745-7794.
36. He F, Tang W, Zhang X, Deng L, Luo J. High energy density solid state lithium metal batteries enabled by Sub-5 μm solid polymer electrolytes. *Adv Mater.* 2021;33(45):2105329.
37. Huo H, Chen Y, Luo J, Yang X, Guo X, Sun X. Rational design of hierarchical “ceramic-in-polymer” and “polymer-in-ceramic” electrolytes for dendrite-free solid-state batteries. *Adv Energy Mater.* 2019;9(17):1804004.
38. Masias A, Felten N, Garcia-Mendez R, Wolfenstine J, Sakamoto J. Elastic, plastic, and creep mechanical properties of lithium metal. *J Mater Sci.* 2019;54(3):2585-2600.
39. Craig RR. *Mechanics of Materials.* Wiley & Sons; 2011.
40. Cook M, Larke EC. Resistance of copper and copper alloys to homogeneous deformation in compression. *J Inst Met.* 1945;71:371-390.
41. Bruce PG, Vincent CA. Steady state current flow in solid binary electrolyte cells. *J Electroanal Chem Interfacial Electrochem.* 1987;225(1-2):1-17.
42. Molinari N, Mailoa JP, Kozinsky B. Effect of salt concentration on ion clustering and transport in polymer solid electrolytes: a molecular dynamics study of PEO-LiTFSI. *Chem Mater.* 2018;30(18):6298-6306.

43. Gouverneur M, Schmidt F, Schönhoff M. Negative effective Li transference numbers in Li salt/ionic liquid mixtures: does Li drift in the “wrong” direction? *Phys Chem Chem Phys*. 2018;20(11):7470-7478.
44. Molinari N, Mailoa JP, Craig N, Christensen J, Kozinsky B. Transport anomalies emerging from strong correlation in ionic liquid electrolytes. *J Power Sources*. 2019;428:27-36.
45. Wang X, Salari M, Jiang D, et al. Electrode material–ionic liquid coupling for electrochemical energy storage. *Nat Rev Mater*. 2020;5(11):787-808.
46. Singh MP, Singh RK, Chandra S. Ionic liquids confined in porous matrices: physicochemical properties and applications. *Prog Mater Sci*. 2014;64:73-120.
47. Zhang S, Zhang J, Zhang Y, Deng Y. Nanoconfined ionic liquids. *Chem Rev*. 2017;117(10):6755-6833.
48. Iacob C, Sangoro JR, Papadopoulos P, et al. Charge transport and diffusion of ionic liquids in nanoporous silica membranes. *Phys Chem Chem Phys*. 2010;12(41):13798-13803.
49. Berrod Q, Ferdeghini F, Judeinstein P, et al. Enhanced ionic liquid mobility induced by confinement in 1D CNT membranes. *Nanoscale*. 2016;8(15):7845-7848.

### SUPPORTING INFORMATION

Additional supporting information can be found online in the Supporting Information section at the end of this article.

**How to cite this article:** Agrawal A, Yari S, Hamed H, Gouveia T, Lin R, Safari M. Synergistic interactions between the charge-transport and mechanical properties of the ionic-liquid-based solid polymer electrolytes for solid-state lithium batteries. *Carbon Energy*. 2023;e355.  
[doi:10.1002/cey2.355](https://doi.org/10.1002/cey2.355)